

RESEARCH LETTER

10.1002/2014GL061844

Key Points:

- The NEA is playing a key role in the global warming hiatus
- The NEA's intermediate and deep layers have warmed in the 2000s decade
- This warming is observed in the subpolar gyre

Correspondence to:

D. G. Desbruyères,
dades@noc.ac.uk

Citation:

Desbruyères, D. G., E. L. McDonagh, B. A. King, F. K. Garry, A. T. Blaker, B. I. Moat, and H. Mercier (2014), Full-depth temperature trends in the northeastern Atlantic through the early 21st century, *Geophys. Res. Lett.*, *41*, 7971–7979, doi:10.1002/2014GL061844.

Received 12 SEP 2014

Accepted 27 OCT 2014

Accepted article online 29 OCT 2014

Published online 26 NOV 2014

Full-depth temperature trends in the northeastern Atlantic through the early 21st century

D. G. Desbruyères¹, E. L. McDonagh¹, B. A. King¹, F. K. Garry², A. T. Blaker¹, B. I. Moat¹, and H. Mercier³

¹National Oceanography Centre, Southampton, UK, ²School of Ocean and Earth Science, University of Southampton, National Oceanography Center, Southampton, UK, ³Laboratoire de Physique des Océans, UMR 6523 CNRS-Ifremer-UBO-IRD, Plouzané, France

Abstract The vertical structure of temperature trends in the northeastern Atlantic (NEA) is investigated using a blend of Argo and hydrography data. The representativeness of sparse hydrography sampling in the basin mean is assessed using a numerical model. Between 2003 and 2013, the NEA underwent a strong surface cooling (0–450 m) and a significant warming at intermediate and deep levels (1000 m to 3000 m) that followed a strong cooling trend observed between 1988 and 2003. During 2003–2013, gyre-specific changes are found in the upper 1000 m (warming and cooling of the subtropical and subpolar gyres, respectively), while the intermediate and deep warming primarily occurred in the subpolar gyre, with important contributions from isopycnal heave and water mass property changes. The full-depth temperature change requires a local downward heat flux of $0.53 \pm 0.06 \text{ W m}^{-2}$ through the sea surface, and its vertical distribution highlights the likely important role of the NEA in the recent global warming *hiatus*.

1. Introduction

The warming of the Earth's climate system is unequivocal and certainly linked to an on-going increase in the concentration of greenhouse gases in the atmosphere [e.g., *Intergovernmental Panel on Climate Change (IPCC)*, 2013]. Since around 2001, a reduction in global surface and subsurface temperature rise has been observed [e.g., *Trenberth and Fasullo*, 2010; *Lyman et al.*, 2010], leading to the hypothesis of internally driven transfers of heat from shallow to deep oceanic layers [*Palmer et al.*, 2011]. While model studies have started to address the potential drivers of such *hiatus* periods, including the role of El-Niño in the Pacific and that of the meridional overturning circulation in the Atlantic [*Meehl et al.*, 2011; *Loeb et al.*, 2012; *England et al.*, 2014], regional and observation-based analyses of the full-depth structure of temperature changes are urgently needed.

Since about 2003, the upper 2000 m of the global ocean have been effectively sampled by Argo profiling floats, giving confidence in the assessment of oceanic heat content (OHC) changes [*Abraham et al.*, 2013]. Between 2005 and 2012, the 10–2000 m layer was shown to warm at a rate of $0.3 \pm 0.1 \text{ W m}^{-2}$ [*von Schuckmann and Le Traon*, 2011], one third of this warming being observed below 700 depth [*Levitus et al.*, 2012]. Deeper in the water column, knowledge of OHC variability is often limited by the spatial and temporal sparseness of in situ observations. Using 28 hydrographic sections from all major ocean basins, *Purkey and Johnson* [2010] reported a global downward heat flux of $0.027 \pm 0.009 \text{ W m}^{-2}$ required to account for their estimated warming rates below the 4000 m interface between the 1990s and 2000s. *Kouketsu et al.* [2011] extended the analysis of *Purkey and Johnson* [2010] on the subregional scale and demonstrated the statistical robustness of hydrographically based OHC estimations below the energetic intermediate layers. Amongst others, these studies highlight the crucial contribution of the intermediate, deep, and abyssal oceanic layers to the global energy and sea level budgets [e.g., *Church et al.*, 2011].

Although there is often a strong focus on the warming of the deep and abyssal Southern Ocean, important regional disparities in the 1990s–2000s deep temperature trends have been revealed [*Purkey and Johnson*, 2010; *Wunsch and Heimbach*, 2014]. A statistically significant cooling of the northeastern Atlantic (NEA hereafter) stood out, contrasting with a warming of its upper layers that followed shifts in the horizontal gyre circulation circa 1995 [*Häkkinen and Rhines*, 2004; *Leadbetter et al.*, 2007]. Deep convection processes at high latitudes constantly renew the properties of intermediate, deep, and abyssal waters in the whole North Atlantic with significant interannual/decadal variations. This makes the North Atlantic a potential candidate for any deep storage of heat [*Kostov et al.*, 2014; *Chen and Tung*, 2014]. We here combine new estimates of temperature changes from Argo and hydrography data to detail the vertical structure of

temperature trends in the NEA during the 1990s–2000s–2010s decades, with a focus on the Argo era (2003–onward). The regional pattern of variability and the relevant oceanic mechanisms (heaving and/or water mass temperature changes) will be quantified, and a numerical model will be used to assess the representativeness of the hydrographic sampling.

The paper is structured as follows. Section 2 presents Argo and hydrography data and provides a description of the numerical model (section 2.3). Decadal changes in the deepest portion of the water column from the late 1980s to the early 2010s are diagnosed from repeat hydrography data in section 3.1 and further assessed in a numerical model in section 3.2. We then focus on the early 21st century (the hiatus years) by combining Argo and hydrography data (section 4) and describe the regional patterns and mechanisms of variability in section 5. Section 6 summarizes the main results.

2. Observational Data Sets and Ocean Model

2.1. Argo

Argo profiling data gathered on a 10 day basis between March 2003 and December 2012 and corrected by the Argo-delayed mode quality control teams are used to compute temperature trends between the sea surface and 1990 m depth. The year 2003 was chosen as the time when the Argo fleet in the North Atlantic became complete. A complete and up-to-date description of Argo data accuracy and biases is provided in *Abraham et al.* [2013]. Optimal interpolation is here used to select and map Argo profiles on a regular 2° grid with a 20 db vertical resolution. The mapping error is related to the sampling distribution and variance of the temperature profiles selected for a given grid point.

The study area extends from the equator to 65°N and is bounded by the Mid-Atlantic Ridge (MAR) and Reykjanes Ridge to the west (thus excluding the Irminger Sea), the Iceland-Scotland sills to the northeast, and the European and African coastlines to the east (see Figure 1). For the present study, the yearly average number of profile within 2° boxes ranges from around 25 circa 2004 to around 50 circa 2011, with maximum float density found between 35°N and 55°N in the subpolar gyre and fewer measurements off Africa and along the southern portion of the MAR.

2.2. Hydrography

The deepest layers of the NEA basin have been effectively sampled along three hydrographic sections during the last two decades: the A25-Ovide line (six repeats), the A16N line (five repeats), and the A05E line (four repeats). Although the focus here is on the 2000s decade, the 1990s repeats will be used to highlight decadal changes in deep temperature trends. The geographical positions and respective dates of occupation for each section are shown in Figure 1. The data used consist of full-depth conductivity-temperature-depth (CTD) profiles of temperature and salinity as a function of pressure (2 db vertical resolution) with standard accuracy of 0.002°C and 0.002 PSS-78, respectively. Each individual profile of in situ temperature is converted to potential temperature referenced to the sea surface (noted θ hereafter). Vertical profiles of θ are then low passed vertically using a 40 db half-width Hanning filter and interpolated onto an evenly spaced 20 db–2' (~3.8 km) vertical-horizontal grid. The distances covered by each section at every pressure level are computed using the ETOPO2.v2 bathymetry product and will be used to weight in the basin-mean average.

2.3. ORCA025

The model simulation used is an integration of NEMO ORCA025 (1/4°) forced with the ERA Interim data set [*Dee et al.*, 2011] for the period from January 1989 to March 2011. It is initialized from a longer integration of the same code forced with the CORE2 interannual forcing data set [*Large and Yeager*, 2004, 2008], so adjustment from the initial state is relatively small compared with starting from rest. The code used is NEMO (Nucleus for European Modelling of the Ocean) v3.2 [*Madec*, 2008], and sea ice is represented by the Louvain-la-Neuve Ice Model version 2 (LIM2) sea ice model [*Timmermann et al.*, 2005]. Both the ERA Interim forced integration and the CORE2 forced integration have been published previously [*Blaker et al.*, 2014].

3. Deep and Abyssal Temperature Trends (1988–2012)

3.1. Repeat Hydrography

The computation of temperature trends from repeat hydrography surveys follows the methodology of *Purkey and Johnson* [2010]. We here focus on the portion of the water column below 2000 m depth due to potentially strong temporal biases in the hydrography sampling within the energetic upper layers. The rate

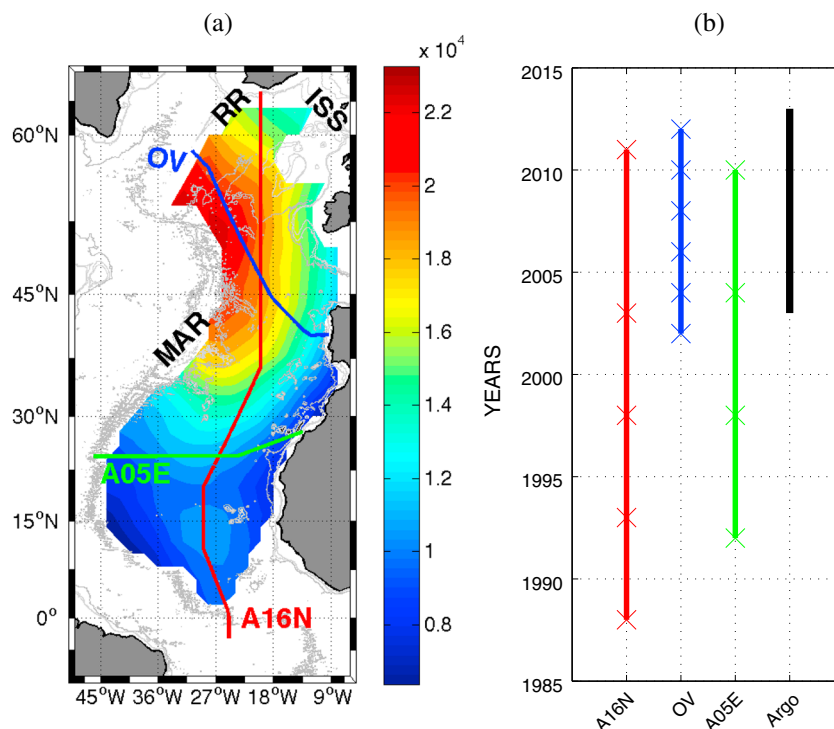


Figure 1. (a) Total number of Argo profiles within the NEA domain as selected by the optimal interpolation between March 2003 and January 2013. The locations of the three hydrographic sections analyzed are shown: A16N (red), A25-Ovide (blue), and A05E (green). The bathymetry features mentioned in the text are labeled as MAR (Mid-Atlantic Ridge), RR (Reykjanes Ridge), and ISS (Island-Scotland sill). (b) The temporal windows covered by the repeat hydrography surveys at each section (crosses indicate the section occupations; same color code as Figure 1a). The Argo window is shown in black.

of change of temperature at every vertical and horizontal grid point along each section is obtained by fitting a straight line to the individual measurements. The pressure-distance fields are then averaged horizontally to provide vertical profiles of temperature trends, with the associated uncertainties depending on the standard deviation at each pressure level (reflecting the spatial homogeneity of temperature trends) and an estimation of the effective degrees of freedom. The latter relies on a characteristic horizontal decorrelation length scale (105 km on average) computed from the autocovariance function of the spatially detrended trends at each pressure level. The number of degrees of freedom is then found by dividing this scale by the length of the section at each pressure level and the 95% intervals estimated using a Student's *t* distribution. Profiles of density and thermal capacity (computed from the Hydrobase 3 climatology) and of the basin area (computed from the ETOPO2.v2 bathymetry) are used to derive the equivalent vertical heat flux required to account for the warming/cooling rate below each pressure level.

Figure 2 shows the pressure-distance sections of long-term temperature trends below 2000 m depth from (a) the five 1988–2011 A16N, (b) the four 1992–2010 A05E, and (c) the six 2002–2010 A25-Ovide cruises. From here we choose 45°N as the limit between subpolar and subtropical regions and define the deep layers from 2000 m to 4000 m and the abyssal layers from 4000 m to the bottom. The 1990s to 2000s picture captured by A16N and A05E is a dominant warming of the deep subtropical region, a cooling of the deep subpolar region and a subtropical abyssal cooling. As shown below, these long-term changes at A16N and A05E primarily describe a 1990s signal. The temperature changes along A25-Ovide, restricted to the 2000s years, show a strong warming over most of the deep subpolar gyre and a fairly weak abyssal warming in the northern subtropics.

A length-weighted average of the three sections at each pressure level yields basin-mean profiles of temperature trends, shown in Figure 3 with the respective contribution of the three sections. To highlight potential decadal changes, linear trends are computed up to and from the year 2000. Moreover, A16N is decomposed into a subpolar (> 45°N, SPG) and a subtropical (< 45°N, SPG) contribution to document the spatial

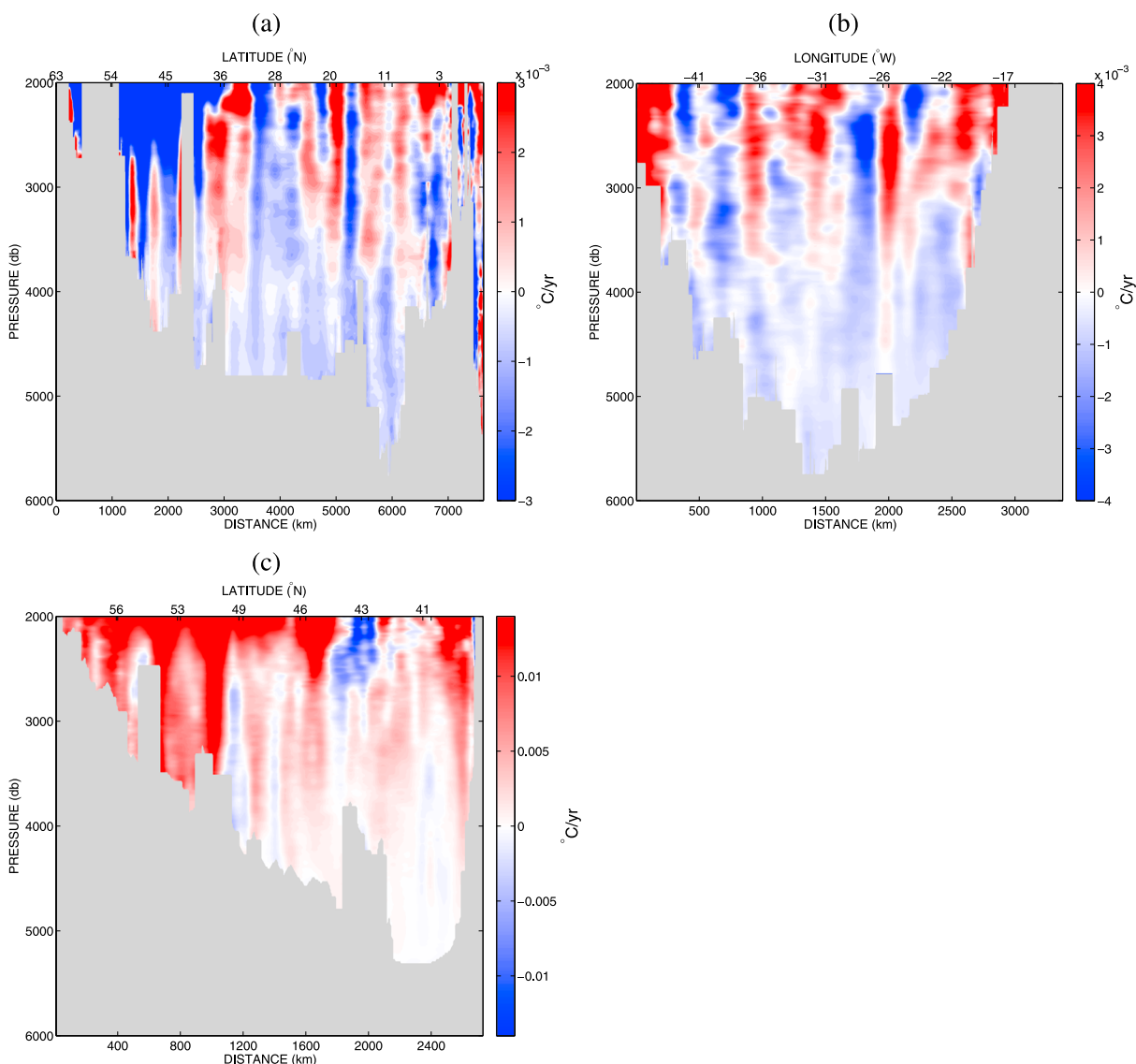


Figure 2. Sections of temperature trend below 2000 m depth computed from (a) the five 1988–2011 A16N, (b) the four 1992–2010 A05E, and (c) the six 2002–2010 A25-Ovide cruises. Units are $^{\circ}\text{C yr}^{-1}$. Note the different scaling.

distribution of the trends. A basin-mean cooling of the deep and abyssal waters in the late twentieth century is revealed (Figure 3a). It reflects a subtropical cooling in the abyss and a strong subpolar cooling at deep levels damped by a warming of the subtropics above 3000 m depth. Noteworthy, this subtropical warming is captured by both A16N STG and A05E and gives confidence in the large-scale representativeness of the hydrographic sampling. The basin-mean temperature change is associated with a vertical heat flux of $-0.79 \pm 0.08 \text{ W m}^{-2}$ and $-0.25 \pm 0.01 \text{ W m}^{-2}$ across the 2000 db and 4000 db isobars, respectively (negative sign meaning upward, no figure shown). The trends at deep levels then reversed in the 2000s (Figure 3b), while the abyssal layers were still cooling but at a much smaller rate ($0.43 \pm 0.05 \text{ W m}^{-2}$ and $-0.01 \pm 0.004 \text{ W m}^{-2}$ across the 2000 db and 4000 db isobars, respectively). The substantial deep warming is found in the subpolar region and is captured here by A25-Ovide only as A16N was not occupied north of 48°N in 2011.

3.2. Representativeness of Deep Hydrography Sampling in ORCA025

The decadal trends derived from repeat hydrography may not be representative of basin average trends because observations are limited in their temporal frequency (typically 2–5 years) and their spatial coverage. Here we analyze a 0.25° resolution NEMO simulation (see section 2.3) for the period 1990–2010 to assess the uncertainty that might surround the trends reported in section 3.1. We note that while adjustment from

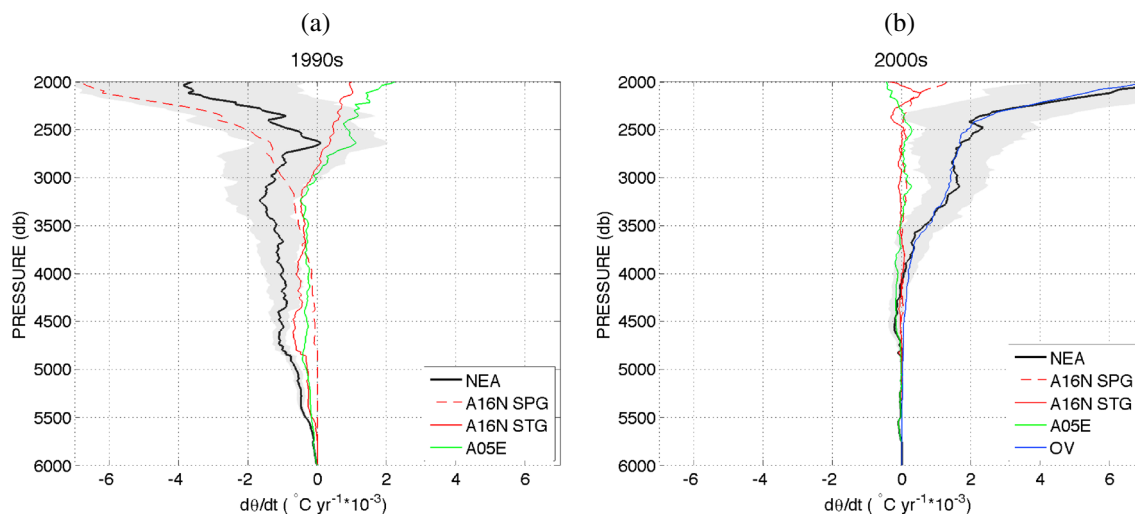


Figure 3. Basin-mean vertical profile of temperature trend below 2000 m depth (black) and length-weighted contributions of A16N (red), A05E (green), and A25-Ovide (blue) during (a) the 1990s and (b) the 2000s. Grey shading indicates 95% confidence intervals (see text for details). Units are $^{\circ}\text{C yr}^{-1}$.

the initial state is relatively small in this integration, the deep ocean will continue to drift. We hence use the model simulation to assess the representativeness of the hydrographic sampling but avoid making direct comparison between the observed and modeled trends.

Subsampling the model output by selecting 5 day mean data along the A16N and A05E sections provides the model truth on sections and enables quantification of likely spatial uncertainty. Selecting model output only for the dates and locations of actual cruises creates pseudosections that represent both

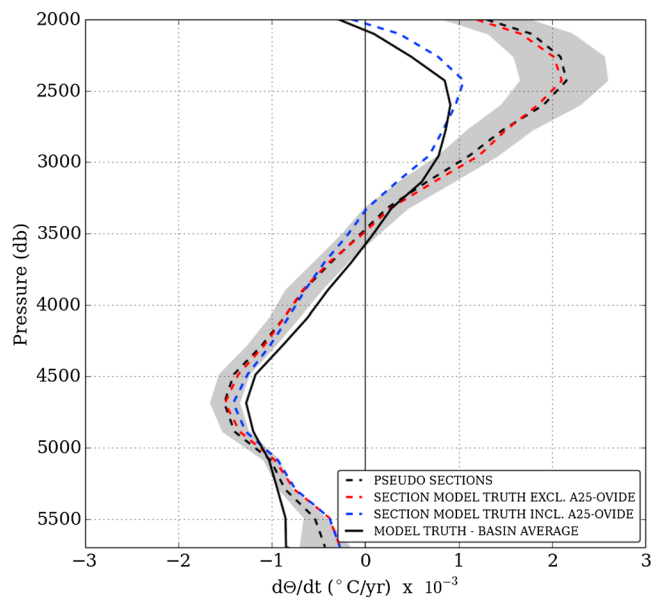


Figure 4. Basin-mean vertical profiles of $d\theta/dt$ (1990–2010) from model output using the NEA basin average (solid line) and the length-weighted section average of A05E and A16N using both the 5 day mean output (red dashed) and pseudosections (black dashed). The shaded area indicates the region between $\pm 2\sigma$ of 1000 alternative pseudosections using randomly selected dates between ± 1 year of the actual cruises. The blue dashed line is $d\theta/dt$ for the length-weighted section average using 5 day mean output along sections A16N, A05E, and A25-Ovide.

the temporal and spatial coverage achieved by actual observations. Temperature trends for each type of data are presented in Figure 4. It indicates that hydrographic sampling that adequately reflects the time period of study is not likely to possess large temporal uncertainty but that significant spatial uncertainty may exist, particularly between 2000 and 3000 m. However, including the comparatively short and shallow A25-Ovide line significantly reduces the spatial uncertainty above 3500 m, indicating that its inclusion in the observational analysis from the year 2000 improves the estimated temperature trends. Overall, our analysis suggests that overall recent observations are likely to have captured temperature trends below 2000 m reasonably well; on average, the cooling trend in the model basin is overestimated by $\sim 20\%$ using observational style sampling. We further quantify the temporal uncertainty associated with the hydrographic data using a Monte

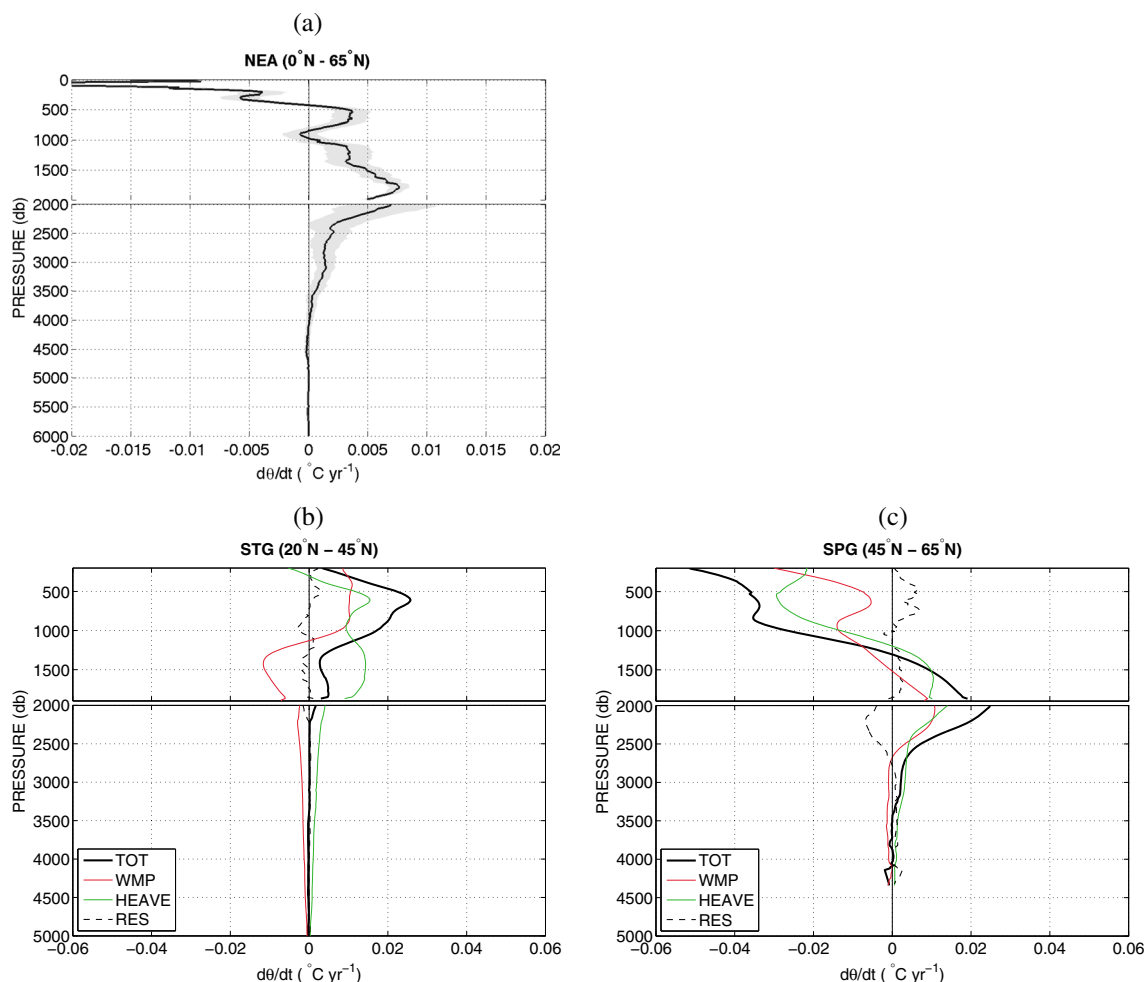


Figure 5. (a) The full-depth profile of temperature trends in the NEA basin during the 2000s from Argo (0–2000 m) and repeat hydrography (2000 m to 5000 m). Grey shading indicates 95% confidence intervals. Units are $^{\circ}\text{C yr}^{-1}$. (b) The total subtropical (20–45°N) profile decomposed into water mass property changes along neutral surfaces (red, WMP) and changes due to the heave of neutral surfaces (green, HEAVE) along with the residual from the true trend (dashed, RES). (c) Same as Figure 5b but for the subpolar subbasin (45–65°N). Note the different x scales used.

Carlo method in which we randomly select alternative cruise dates within ± 12 months of the cruise to generate 1000 alternative pseudosections. The shaded area in Figure 4 represents ± 2 standard deviations of the alternative pseudosections and demonstrates the relatively small temporal uncertainty that could arise due to scheduling of cruises or delays due to weather.

4. The Full-Depth Picture From Argo and Hydrography (2003–2012)

The three-dimensional gridded field of temperature anomalies based on the optimal interpolation of Argo profiles is used to estimate the 2003–2012 linear trend above 2000 m depth. At each grid point, the rate of change of temperature is obtained by fitting a straight line within the 10 year time series using a least squares approach. The associated error at each time step is chosen as the maximum of the mapping error and the residual between the linear fit and the actual signal, and the 95% interval is estimated using a Student's t distribution. A horizontal average at each pressure level yields a vertical profile of temperature trend for the top 2000 m of the water column (Figure 5a), which is combined with the corresponding 2000s hydrography-based profile below 2000 m previously shown in Figure 3b.

The Argo-based profile shows a cooling of the upper 450 m and a warming of the 450 m to 2000 m layer peaking at about 1800 m, suggesting that advection rather than mixing is playing a primary role (Figure 5a). The integrated effects of these two signals are of similar magnitude, and the resulting contribution of the

0–2000 m layer to the regional heat and sea level budgets is a relatively small downward heat flux across the sea surface of $0.1 \pm 0.01 \text{ W m}^{-2}$ and a drop in sea level of $-0.22 \pm 0.03 \text{ mm yr}^{-1}$. Merging the 0–2000 m Argo profile with the 2000 m to 6000 m hydrography profile yields an average warming rate of the whole water column of $6.6 \times 10^{-4} \text{ }^\circ\text{C yr}^{-1}$, corresponding to a downward heat flux of $0.53 \pm 0.06 \text{ W m}^{-2}$ through the sea surface and a thermometric sea level rise of $0.29 \pm 0.09 \text{ mm yr}^{-1}$. Overall, it is found that the intermediate and deep layers of the NEA (between 450 m and 4000 m depth) have significantly warmed in the early 2000s, with a warming peak in the depth range of Labrador Sea Water. Its overall effect on the heat content of the basin was damped by a major and minor cooling of its surface/subsurface (0–450 m) and abyssal (4000 m–bottom) layers, respectively.

5. Mechanisms of Variability (2003–2012)

We now examine the mechanisms responsible for the reported trends within two latitudinal bands: the subtropics (20–45°N) and the subpolar regions (45–65°N). These two particular regions are frequently distinguished in the literature due to their distinct dynamics and subsequent responses to large-scale atmospheric forcing [e.g., Lozier *et al.*, 2008; Mauritzen *et al.*, 2012]. Note that temperature changes within the tropical band (0–20°N), which are not described here, have a fairly small contribution to the basin-mean trend in the top 2000 m layer (not shown). Following Bindoff and McDougall [1994], the reported trend at each pressure level is decomposed into (1) water mass property changes on neutral surfaces and (2) changes due to vertical heave of neutral surfaces, following equation (1):

$$\left. \frac{d\theta}{dt} \right|_p = \left. \frac{d\theta}{dt} \right|_n - \left. \frac{dp}{dt} \right|_n \left(\frac{\partial\theta}{\partial p} \right) \quad (1)$$

where $\left. \frac{d\theta}{dt} \right|_p$ denotes changes along pressure surfaces and $\left. \frac{d\theta}{dt} \right|_n$ denotes changes along neutral surfaces. This decomposition identifies the relative contribution of diabatic processes (e.g., local or remote changes of surface buoyancy fluxes) and adiabatic displacements of the water column (e.g., wind-driven dynamics) to the observed temperature trends. Figure 5 shows the reconstructed profiles of subtropical (Figure 5b) and subpolar (Figure 5c) temperature trends along with the respective contribution of mechanisms (1) and (2), from both Argo (0–2000 m) and hydrography data (2000 m to 6000 m). Despite small discrepancies (notably at thermocline levels where strong vertical gradients are generally found), the overall vertical structure and magnitude of the trends is well captured by equation (1).

The subtropical and subpolar regions exhibit opposing trends above about 1200 m depth where they respectively warmed (subsurface intensified) and cooled (surface intensified), with a similar contribution of mechanisms (1) and (2). Note that the amplitude of the trends is about 2 times larger in the subpolar region than farther south, in agreement with the spatial pattern and magnitude of sea surface height variability seen in altimetry data [Häkkinen *et al.*, 2013]. Below about 1200 m depth, the two mechanisms compensate themselves in the subtropical gyre, leading to a relatively small warming at constant depth, while they both contribute to significantly warm the subpolar region between 1500 m and 2500 m depth, a depth layer primarily occupied by Labrador Sea Water. We observe a cooling along neutral surface in the abyssal subtropical gyre potentially reflecting a change in the properties of Antarctic Bottom Water. Its very small magnitude, however, prevents any strong assertion of its robustness. To conclude, the basin-mean profile of temperature trend is shaped by a surface cooling in the subpolar gyre, opposing gyre-specific signals of large amplitude at subsurface levels, and a significant warming of the intermediate layers in the subpolar gyre. Both the heave of neutral surfaces and the actual changes in water mass properties have an important signature at subpolar and subtropical latitudes.

6. Discussion and Conclusions

While previous observational studies have highlighted a surface-intensified warming pattern of the global ocean [Levitus *et al.*, 2012] and a broad warming of its deep and abyssal layers spreading north from the Southern Ocean [Purkey and Johnson, 2010], our analysis highlights the peculiar behavior of the northeastern Atlantic basin through the early 21st century. Using a combination of repeat hydrography and Argo float measurements, this basin was shown to undergo a surface cooling, a significant warming at intermediate and deep levels, and a comparatively small cooling of its abyssal layers. The overall warming

signal of the intermediate and deep layers dominates the full-depth signal and reflects a striking reversal of a significant cooling trend observed between the late 1980s and the late 1990s [Johnson *et al.*, 2005].

The full-depth 2000s basin-mean trends are of particular interest for a better understanding of the recent change in oceanic heat storage. The first kilometer of the water column shows a gyre-specific response, with a cooling of the subpolar gyre and a warming of the subtropical gyre, respectively, peaking and dominating the basin-mean profile at surface and subsurface levels. It is noteworthy that the cooling trend in the eastern subpolar gyre is consistent with a weakening of the oceanic heat transport reported across the A25-Ovide section during the 2000s years [Mercier *et al.*, 2013]. Below the main thermocline, both Argo and hydrography data reveal a significant warming of the Labrador Sea Water (LSW) depth range (1000–3000 m) in the subpolar gyre, and relatively minor changes at subtropical latitudes. This pronounced decadal change is consistent with a cold-to-warm shift of LSW from the mid-1990s to the early 2000s in the Labrador Sea [Yashayaev *et al.*, 2007], reaching the eastern basins after a few years of advection within the North Atlantic Current [Bersh, 2002]. Applying the decomposition of Bindoff and McDougall [1994] shows that both temperature changes along neutral surfaces and their vertical displacements are equally important in driving temperature trends at constant depth in the NEA basin. Neutral surfaces above about 1500 m depth were mainly uplifted in the subpolar region and depressed in subtropical regions, that is a cooling and warming at constant depth, respectively. This heaving effect was augmented by water mass property changes along neutral surfaces, except in the intermediate and deep subtropical area where the two mechanisms were found to oppose each other. Lastly, the slight (hence questionable) abyssal cooling revealed by the repeat hydrography was mainly observed in the subtropical region where the northward flowing Antarctic Bottom Water is found.

From a heat budget perspective, our estimation of full-depth temperature changes in the NEA during the early 21st century requires a downward heat flux through the sea surface of $0.53 \pm 0.06 \text{ W m}^{-2}$ and thermometric sea level rise of $0.30 \pm 0.08 \text{ mm yr}^{-1}$, which respectively equates to $0.016 \pm 0.001 \text{ W m}^{-2}$ and $0.008 \pm 0.001 \text{ mm yr}^{-1}$ when considering the whole area of the Earth. This would explain about 3% of the $\sim 0.6 \text{ W m}^{-2}$ energy imbalance resulting from anthropogenic forcing in the 2000s [Allan *et al.*, 2014]. Most importantly, the vertical distribution of temperature changes clearly demonstrates the need to analyze the whole water column when discussing the energy budget of the climate system, as widely suggested by the modeling community [e.g., Meehl *et al.*, 2011; Palmer and McNeall, 2014; Wunsch and Heimbach, 2014]. In particular, the post-2000 surface/subsurface cooling overlying a deep-reaching warming confirms the likely important role played by the North Atlantic Ocean's internal variability in the global warming hiatus [Chen and Tung, 2014].

Acknowledgments

This work is a contribution to the DEEP-C project, funded by the British National Environmental Research Council (NERC-grant NE/K004387/1). CTD data were made available by data originators either as public data on the CCHDO website (<http://cchdo.ucsd.edu>), where cruise participants can be identified or directly by cruise PIs. The A25-Ovide cruises were funded by Ifremer, CNRS, INSU and CSIC, and the CARBOCEAN and CARBOCHANGE FP7 projects. Argo data were collected and made freely available by the International Argo Program and the national programs that contribute to it (<http://www.argo.ucsd.edu>, <http://argo.jcommops.org>). The Argo Program is part of the Global Ocean Observing System.

Meghan Cronin thanks two anonymous reviewers for their assistance in evaluating this paper.

References

- Abraham, J. P., et al. (2013), A review of global ocean temperature observations: Implications for ocean heat content estimates and climate change, *Rev. Geophys.*, *51*, 450–483, doi:10.1002/rog.20022.
- Allan, R. P., C. Liu, N. G. Loeb, M. D. Palmer, M. Roberts, D. Smith, and P.-L. Vidale (2014), Changes in global net radiative imbalance 1985–2012, *Geophys. Res. Lett.*, *41*, 5588–5597, doi:10.1002/2014GL060962.
- Bersh, M. (2002), North Atlantic Oscillation-induced changes of the upper layer circulation in the northern North Atlantic Ocean, *J. Geophys. Res.*, *107*(C10), 3156, doi:10.1029/2001JC000901.
- Bindoff, N. L., and T. J. McDougall (1994), Diagnosing climate change and ocean ventilation using hydrographic data, *J. Phys. Oceanogr.*, *24*, 1137–1152.
- Blaker, A. T., J. J.-M. Hirschi, G. McCarthy, B. Sinha, S. Taws, R. Marsh, B. A. de Cuevas, S. G. Alderson, and A. C. Coward (2014), Historical analogues of the recent extreme minima observed in the Atlantic meridional overturning circulation at 26N, *Clim. Dyn.*, doi:10.1007/s00382-014-2274-6.
- Chen, X., and K.-K. Tung (2014), Varying planetary heat sink led to global-warming slowdown and acceleration, *Science*, *345*(6199), 897–903, doi:10.1126/science.1254937.
- Church, J. A., N. J. White, L. F. Konikow, C. M. Domingues, J. G. Cogley, E. Rignot, J. M. Gregory, M. R. van den Broeke, A. J. Monaghan, and I. Velicogna (2011), Revisiting the Earth's sea-level and energy budgets from 1961 to 2008, *Geophys. Res. Lett.*, *38*, L18601, doi:10.1029/2011GL048794.
- Dee, D. P., et al. (2011), The ERA-Interim reanalysis: Configuration and performance of the data assimilation system, *Q. J. R. Meteorol. Soc.*, *137*(656), 553–597.
- England, M. H., S. McGregor, P. Spence, G. A. Meehl, A. Timmermann, W. Cai, A. S. Gupta, M. J. McPhaden, A. Purich, and A. Santoso (2014), Recent intensification of wind-driven circulation in the Pacific and the ongoing warming hiatus, *Nat. Clim. Change*, *4*, 222–227, doi:10.1038/nclimate2106.
- Häkkinen, S., and P. B. Rhines (2004), Decline of the subpolar North Atlantic circulation during the 1990s, *Science*, *304*(5670), 555–559, doi:10.1126/science.1094917.
- Häkkinen, S., P. B. Rhines, and D. L. Worthen (2013), Northern North Atlantic sea surface height and ocean heat content variability, *J. Geophys. Res. Oceans*, *118*, 3670–3678, doi:10.1002/jgrc.20268.

- Intergovernmental Panel on Climate Change (IPCC), C. C. . T. P. S. B. (2013), *Intergovernmental Panel on Climate Change (IPCC), Climate Change 2013: The Physical Science Basis*, Cambridge Univ. Press, Cambridge, U. K.
- Johnson, G. C., J. L. Bullister, and N. Gruber (2005), Labrador Sea Water property variations in the northeastern Atlantic Ocean, *Geophys. Res. Lett.*, *32*, L07602, doi:10.1029/2005GL022404.
- Kostov, Y., K. C. Armour, and J. Marshall (2014), Impact of the Atlantic meridional overturning circulation on ocean heat storage and transient climate change, *Geophys. Res. Lett.*, *41*, 2108–2116, doi:10.1002/2013GL058998.
- Kouketsu, S., et al. (2011), Deep ocean heat content changes estimated from observation and reanalysis product and their influence on sea level change, *J. Geophys. Res.*, *116*, C03012, doi:10.1029/2010JC006464.
- Large, W., and S. Yeager (2004), Diurnal to decadal global forcing for ocean and sea-ice models: The datasets and flux climatologies, *NCAR Tech. Note NCAR/TN-460+STR*, Natl. Cent. for Atmos. Res., Boulder, Colo.
- Large, W. G., and S. Yeager (2008), The global climatology of an interannually varying air-sea flux data set, *Clim. Dyn.*, *33*(2–3), 341–364.
- Leadbetter, S. J., R. G. Williams, E. L. McDonagh, and B. A. King (2007), A twenty year reversal in water mass trends in the subtropical North Atlantic, *Geophys. Res. Lett.*, *34*, L12608, doi:10.1029/2007GL029957.
- Levitus, S., et al. (2012), World ocean heat content and thermosteric sea level change (0–2000 m), 1955–2010, *Geophys. Res. Lett.*, *39*, L10603, doi:10.1029/2012GL051106.
- Loeb, N. G., J. M. Lyman, G. C. Johnson, R. P. Allan, D. R. Doelling, T. Wong, B. J. Soden, and G. L. Stephens (2012), Observed changes in top-of-atmosphere radiation and ocean heat content consistent with uncertainty, *Nat. Geosci.*, *5*, 110–113.
- Lozier, M. S., S. Leadbetter, R. G. Williams, V. Roussenov, M. S. C. Reed, and N. J. Moore (2008), The spatial pattern and mechanisms of heat-content change in the North Atlantic, *Science*, *319*(5864), 800–803, doi:10.1126/science.1146436.
- Lyman, J. M., S. A. Good, V. V. Gouretski, M. Ishii, G. C. Johnson, M. D. Palmer, D. M. Smith, and J. K. Willis (2010), Robust warming of the global upper ocean, *Nature*, *465*, 334–337, doi:10.1038/nature09043.
- Madec, G. (2008), NEMO Ocean engine, *Tech. Rep.*, *27*, Institut Pierre-Simon Laplace (IPSL), France.
- Mauritzen, C., A. Melsom, and T. Sutton (2012), Importance of density-compensated temperature change for deep North Atlantic Ocean heat uptake, *Nat. Geosci.*, *5*, 905–910, doi:10.1038/ngeo1639.
- Meehl, G. A., J. M. Arblaster, J. T. Fasullo, A. Hu, and K. E. Trenberth (2011), Model-based evidence of deep-ocean heat uptake during surface-temperature hiatus periods, *Nat. Clim. Change*, *1*, 360–364, doi:10.1038/NCLIMATE1229.
- Mercier, H., P. Lherminier, A. Sarafanov, F. Gaillard, N. Daniault, D. Desbruyères, A. Falina, B. Ferron, C. Gourcuff, T. Huck, and V. Thierry (2013), Variability of the meridional overturning circulation at the greenland-portugal ovide section from 1993 to 2010, *Prog. Oceanogr.*, doi:10.1016/j.pocean.2013.11.001.
- Palmer, M. D., and D. J. McNeall (2014), Internal variability of Earth's energy budget simulated by CMIP5 climate models, *Environ. Res. Lett.*, *9*, 034016, doi:10.1088/1748-9326/9/3/034016.
- Palmer, M. D., D. J. McNeall, and N. J. Dunstone (2011), Importance of the deep ocean for estimating decadal changes in Earth's radiation balance, *Geophys. Res. Lett.*, *38*, L13707, doi:10.1029/2011GL047835.
- Purkey, S. G., and G. C. Johnson (2010), Warming of global Abyssal and deep Southern Ocean waters between the 1990s and 2000s: Contribution to global heat and sea level rise budgets, *J. Clim.*, *23*, 6336–6350, doi:10.1175/2010JCLI3682.1.
- Timmermann, A., H. Goosse, G. Madec, T. Fichefet, C. Ethe, and V. Dulire (2005), On the representation of high latitude processes in the ORCA-LIM global coupled sea-ice ocean model, *Ocean Model.*, *8*, 175–201.
- Trenberth, K. E., and J. T. Fasullo (2010), Tracking Earth's energy, *Science*, *328*, 316–317.
- von Schuckmann, K., and P.-Y. Le Traon (2011), How well can we derive global ocean indicators from Argo data?, *Ocean Sci.*, *7*, 783–791.
- Wunsch, C., and P. Heimbach (2014), Bidecadal thermal changes in the abyssal ocean, *J. Phys. Oceanogr.*, *44*, 2013–2030, doi:10.1175/JPO-D-13-096.1.
- Yashayaev, I., M. Bersh, and H. M. van Aken (2007), Spreading of the Labrador Sea Water to the Irminger and Iceland basins, *Geophys. Res. Lett.*, *34*, L10602, doi:10.1029/2006GL028999.